Design and performance of a test rig for evaluation of nanopositioning stages

OPEN ACCESS
IOP Publishing
Measurement Science and Technology
Meas. Sci. Technol. **30** (2019) 035002 (10pp)
https://doi.org/10.1088/1361-6501/aafd03

Design and performance of a test rig for evaluation of nanopositioning stages

Andrew Yacoot[1], Petr Klapetek[2,3], Miroslav Valtr[2], Petr Grolich[2], Herve Dongmo[1], Giovanni M Lazzerini[1] and Angus Bridges[1]

[1] National Physical Laboratory, Hampton Road, Teddington, Middlesex, TW11 0LW, United Kingdom
[2] Czech Metrology Institute, Okružní 31, 638 00 Brno, Czechia
[3] CEITEC, Brno University of Technology, Purkyňova 123, 612 00 Brno, Czechia

E-mail: andrew.yacoot@npl.co.uk

Received 6 September 2018, revised 13 December 2018
Accepted for publication 9 January 2019
Published 7 February 2019

Abstract

Nanopositioning stages are used in many areas of nanotechnology and advanced materials analysis, often being integrated into analytical devices such as scanning probe and optical microscopes and manufacturing devices (e.g. lithographic systems). We present a metrological instrument, together with software, designed for traceable evaluation of stage performance. The system capabilities and performance are illustrated by measurement of stages of different levels of accuracy, including a low cost custom built stage manufactured by 3D printing. The traceability of the system is described and main uncertainty sources are discussed. Guidelines are given for the specification of stage performance.

Keywords: multi-axis positioning stages, traceability, nanopositioning, dimensional metrology

(Some figures may appear in colour only in the online journal)

1. Introduction

The last decade has seen an increasing demand for dimensional nanometrology, Leach *et al* (2011) following the predictions of Taniguchi (1983) and hence nanopositioning stages. This has been partially met by commercial stages; a simple internet search will reveal a large number of commercially available stages that operate either in open or closed loop. The latter are servo controlled, usually with capacitance sensors, strain gauges or grating encoders as the displacement sensor. In some applications requiring the highest level of traceability for the measurement of the stage position, optical interferometers are used giving direct traceability to the metre; Lazar *et al* (2009), Gillmer *et al* (2014) and Lee *et al* (2014). The combination of nanopositioning and optical interferometry is very powerful and has led to the development of bespoke nanopositioning systems, Manske *et al* (2007), Liu *et al* (2010) and Manske *et al* (2012). Many of these systems designed for long range movements and have been reviewed by Torralba *et al* (2016) when considering their two dimensional stage design. However, such systems are probably beyond the reach of many users and have a level of complexity that for many applications is not required. Worryingly, there seems to be no standard format for specifying stage performance. For those interested in making traceable measurements with known uncertainty there is an immediate requirement to characterise the performance of the stage in terms of accuracy and uncertainty in the configuration in which the stage will be used, which may well be different from the conditions under which any calibration by the manufacturer was performed. This includes both the position and angular errors, and becomes a more complex problem where multi-axis stages are to be considered. Some work has been done on this in the past, (Xu *et al* 2008), (Klapetek *et al* 2011), using atomic force microscope calibration gratings which is a useful method for AFM systems. However, it offers only a very limited number of points from which to construct an error map and it is difficult to separate grating errors from stage errors; gratings may have errors in the positioning of the individual holes, and for a good stage these errors can be a significant contribution to the uncertainty. While it is possible to calibrate the grating, this is usually done using optical diffraction which gives a global value for grating parameters;

local values can only be obtained if the grating is calibrated using a metrological atomic force microscope. Even then, for a complete analysis, accurate repositioning of the grating on the stage is necessary for a complete study.

In many cases the user does not need to measure traceably the stage performance every time the stage is used. What is required is an assessment or characterisation of the stage performance that, if necessary, could be repeated at regular intervals. A motivation for this work was the requirement for stage characterisation within the growing field of nanotechnology, and particularly for microscopes that did not have on board interferometers, Yacoot *et al* (2007), Corbett *et al* (2018). The solution proposed here for stage characterisation is a dedicated traceable test rig as constructed by the National Physical Laboratory (NPL) and the Czech Metrology Institute (CMI). This has been designed with a flexible configuration to accommodate a wide variety of stages. The concept of the rig is simple: simultaneous measurement of position and angular errors using interferometers and auto collimators in a configuration as near as identical as possible to that in which the stage will be used. Measurements can be made in the same plane as that which will be used away from the test rig, thereby giving a measure of the effect of the Abbe errors on position, which is easily visualised using the vector display approach presented here.

There are many producers of nano and micro positioning stages, meeting different industrial needs via many different products. There are several basic spatial parameters of the stages that relate to performance. The first is the number of scanning axes, one, two or three, possibly combined with angular motion as well. The scan range for most nanopositioning stages varies from the micrometre range up to hundreds of micrometres, although some stages have ranges of millimetres, Manske *et al* (2007), Liu *et al* (2010). The ultimate resolution of a stage operating in closed loop will be governed by the resolution of the actuator generating the motion together with the sensors and feedback electronics in the stage and stage controller, leading to the positioning resolution claimed by manufacturer.

In most cases the positioning stage comprises a guidance mechanism, an actuator to generate motion (e.g. piezo actuator, voice coil or motor), and a sensor to measure generated motion and provide a signal for closed loop control that is usually done with a proportional-integrative-differential (PID) loop implemented in hardware or software. The guidance mechanism can be dovetail, roller bearing, air bearing or flexure based, the actuator usually consists of a piezoelectric stack or voice coil for longer range and the displacement sensor is usually based on capacitance or strain sensors, grating encoders or, as mentioned previously, optical interferometers. Nearly all combinations of the above can be found on the market as all the various options have many advantages and disadvantages depending on the particular application.

Multi axis positioning stages are complex devices, which leads to a number of possible error sources: scale error, linear guidance system errors, cross-talk and angular errors. Most of the potential stage errors will be further defined and discussed later in the paper and an approach for the characterisation of these errors using the test rig will be presented.

2. Experimental arrangements

2.1. Test rig

The Stage Test Rig uses three NPL plane mirror differential optical interferometers (Yacoot and Downs 2000) to measure the displacement of a translation stage in all three axes. In the case of a one or two axis stage, the interferometers associated with the non-moving axes measure only out of plane motion. Two dual-axis autocollimators, built and calibrated at CMI, are used to measure the angular movements associated with the stage. The data is then used to construct a 3D map of the errors associated with the stage which is directly traceable to the SI metre.

The body of the stage rig is constructed from a mixture of off the shelf components and purpose-made supports to allow ease of mounting of a variety of stages. In each case a precision cube mounted on the stage acts as the moving mirror for the interferometers. The cube's orthogonality is 5 microradians (1 s of arc) and each surface has a flatness of lambda/8 at 633 nm over 80% of the 25 mm $\times$ 25 mm face.

The rig is mounted on an anti-vibration platform in a thermal enclosure. The temperature in the laboratory is maintained at 20 °C $\pm$ 0.1 °C. Within the enclosure there is typically a factor of 10 improvement, giving a stability of 10 mK. All measurements are made at 20 °C so that they are in compliance with ISO 1:2016.

The differential configuration of the optical interferometers further reduces the effect of any large scale environmental fluctuations as the measurement and reference beams of the interferometers pass through a common path. Environmental conditions inside the enclosure are monitored and an Edlén correction is applied Birch and Downs (1993, 1994) to the interferometer data to take into account variations in refractive index and reduce errors associated with the interferometer dead paths. Data is sampled at 700 kHz and sub sampled according to the measurement requirements. A real time Heydemann correction (Heydemann 1981, Birch 1990) is applied to minimise interferometer non-linearity.

The autocollimators are based on a position sensitive detector (Hamamatsu S5990-01, photosensitive area of $4 \times 4\,\mathrm{mm}^2$), a laser module with focusing optics (Thorlabs CPS196), a custom built preamplifier (based on TL074 operational amplifier) and divider boards (each based on the AD633 analogue multiplier). Each autocollimator monitors two axes, so there is some redundant information in the data, which was selected to be the stage yaw (z axis rotation) that was expected to be highest angular error component in the 2D and 3D stages. Using different levels of amplification of the signal in the electronics rotation errors can be measured in the range up to 3 milliradians (coarse scale) and with lowest uncertainty of 0.2 microradians (finest scale).

A CAD drawing of the whole instrument is shown in figure 1. The system control allows the operator to select movement range and resolution for a variety of stages. Routines for additional stages can be easily added to the program. The time required for data collection is dependent on the number of lines scanned, the number of pixels per line

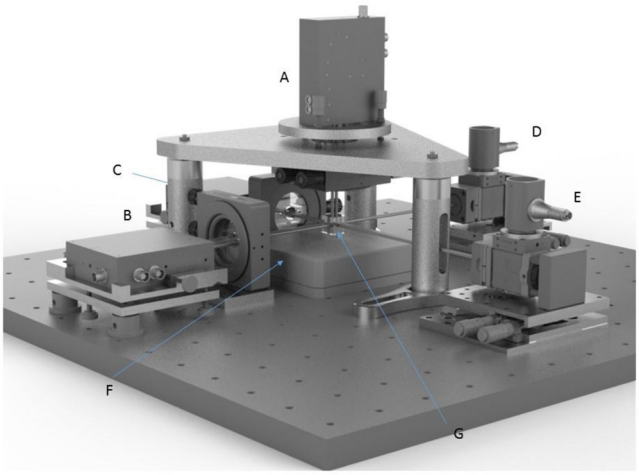

Figure 1. CAD drawing of test rig showing three interferometers, (A) *Z* axis, (Y) *Y* axis, (C) *X* axis, (D) autocollimator for *X* axis, (E) autocollimator for *Y* axis, (F) stage under test, (G) precision cube. Note beam paths for interferometers and autocollimators are also shown.

and the settling time chosen between data points. Sources of uncertainty arising from fluctuations in ambient conditions are time-dependent so data collection time is an important consideration in the measurement strategy.

An important consideration is the mounting and alignment of stages. Stages are mounted to be orthogonal to the system, based on the stage frame. The precision cube is placed on the stage and aligned parallel to the fast (*X*) axis of the stage. There is always some residual angular error which is discussed in the uncertainties section.

2.2. Commercial stages

We have examined three commercially available stages (with one dimensional, two dimensional and three dimensional motion respectively), together with their respective controllers, from three different major manufacturers. To compare the particular stages is not the intention of this paper; we aim to show the range of errors and other effects that can be measured, as well as demonstrating the errors in the different types of stage. Moreover, one stage was over 15 years old, and two were new, so it would be an unfair comparison. Since all stages were designed to be operated in closed loop, they were measured in closed loop.

Stage manufacturers usually claim some typical or maximum stage errors in the datasheets, however the information about how these values were measured or conditions under which they were measured is very limited. The claimed linearity ranged from 0.01 to 0.03% for the stages tested, and angular errors (if given) were specified as being up to 10 μrad (in one case it was 25 μrad for the *z* axis rotations). No orthogonality errors were reported in the datasheets. Where the stage performance in the mode used here deviated from the manufacturer's data sheet we have indicated this, so as to highlight how the stage performance may vary from the manufacturer's calibration depending on the operating conditions.

2.3. Custom built plastic stage

A simple 2D stage was manufactured using a low cost 3D printer (Prusa i3) to have an example of a poor performance system that can still be used for nanopositioning. The stage is based on a 2D flexure linear guidance system as shown in figure 2. Two piezoelectric transducers with fitted strain gauges (Thorlabs PZS001) were used to move the stage. To make it a simple low cost system, an Arduino Due microcontroller was used for controlling the stage, including the feedback loop. High voltage amplifiers based on Apex Microtechnology PA88U circuits were used to feed the transducers. To read the strain gauges AMP002 preamplifier boards from Thorlabs were used. The main limiting factors for the accuracy was the plastic construction which limits stage rigidity along with the use of 12 bit analogue-digital (AD) and digital-analogue (DA) converters on the Arduino. Despite these limitations the stage was successfully used for atomic force microscopy measurements, and has in principle all the features of a nanopositioning stage. The scan range as based on the design and strain gauge outputs is approximately $12 \times 12\ \mu m^2$.

3. Data processing

3.1. Definitions and conventions

In the datasheets of most stages, the measurand is incompletely defined. Since we want to map the stage errors we need to introduce some convention regarding orientation of errors and naming of the angles. As there is no industry standard on this, we need to define some conventions for this paper.

We concentrate mostly on static stage performance, so the error is evaluated after the stage had moved to predetermined positions. Dynamic effects can also be measured, as discussed later, however their meaning and practical impact depends highly on the stage type (sensors and feedback method) and on the application. The static errors can be divided into the following groups.

- Stage scale error: the stage measures its displacement incorrectly due to an incorrect calibration of the internal sensors or a calibration that is no longer valid.
- Stage axes rotational error: the stage could be manufactured to have the axes slightly rotated with respect to the stage frame. Within the test rig we can only align the stage based on its frame as we cannot see what is inside. Although with a series of measurements we could assess any misalignment, for practical purposes, a user is likely to take one of the edges of the stage frame as a reference so for consistency, this is the approach adopted here.
- Stage cross-talk: parasitic motion in one axis if the stage is moved in a second axis, mostly encountered on open loop stages. In addition if the stage axes themselves are not perpendicular, this will appear as a crosstalk term with respect to the interferometer axes.
- Stage hysteresis: present mainly in open-loop stages, is the dependence of the position on the history of the stage motion.

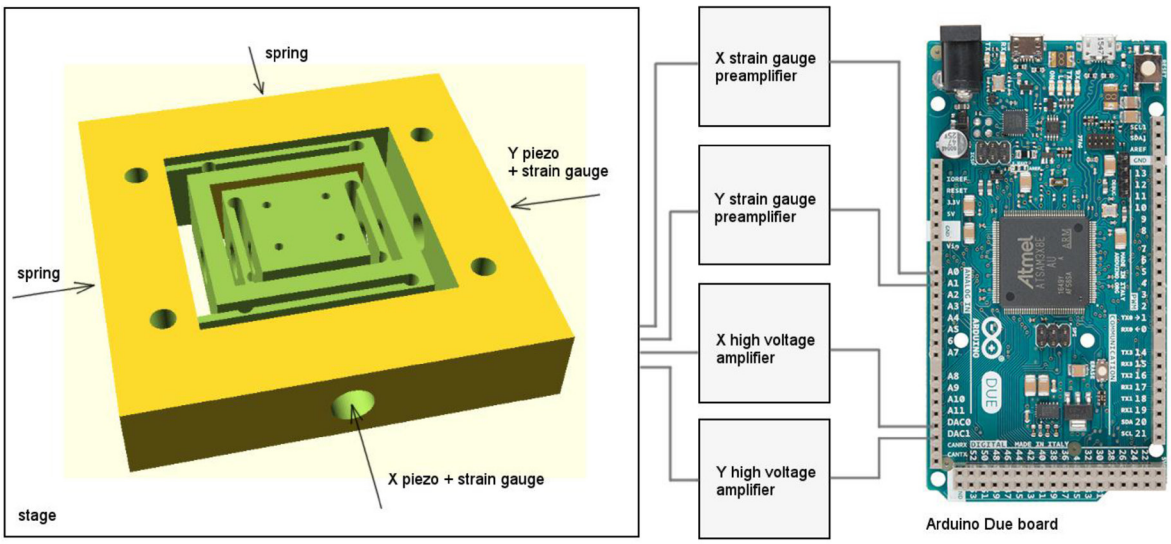

Figure 2. Plastic stage design and control loop.

- Mechanical response errors: while stage is loaded its behaviour can be different from when it is free of any load.

We are evaluating a difference between the desired stage motion (what we request from stage) and real stage motion (what we measure with the interferometer). This is evaluated in a set of positions spanning the stage range and equally distributed across the range. At every position, we obtain a local data set comprising nine values: (x, y, z positions as reported from stage, x, y, z positions as reported by the interferometers, and stage rotation angles: pitch, roll and yaw as reported by the two autocollimators). If the stage is able to move in three dimensions we therefore obtain a 3D array of these local data sets. The most natural way to output these data is in a form of 3D matrices, depending on stage type. This is not, however, a way to present the data to the user for easy visualization of the stage errors - we need some cross-sections or subsets of the data to be defined in order to be able to visualise the data. The following conventions were selected for data treatment and presentation.

- A right handed coordinate system is used, which is the convention for most commercial stages.
- For 2D and 3D stages, the fastest axis is the x axis, according to the manufacturer's notation, z is the slowest axis.
- Cross-sections of data are presented in which the z axis position has been kept constant.
- Stage errors are defined as error as (stage value—interferometer value). This means that if the stage reports as it moved further than it actually did, it is a positive error.
- x, y, z errors are evaluated each separately (calculating e.g. *x-stage* position–*x-interferometer* position at every position, etc)
- The interferometers absolute value offset is set to have the zero error at the centre of the stage motion so the errors are zero at the centre by definition.
- The rotational errors are defined as shown in figure 3. Terms 'stage pitch', 'stage roll' and 'stage yaw' refer to the stage x axis orientation (or the only axis in case of the 1D stage).

The easiest visualisation using the above assumptions is to use a set of 2D false colour or contour maps, coming from Gwyddion open source software (http://gwyddion.net). Figure 4(a) shows such a map for x, y and z error for a simulated stage data with relatively complex positioning errors.

The x, y and z error information can also form a 3D vector, so the data can be visualised as a map of arrows in 3D as shown in figure 4(b). This simultaneously shows the errors in all three axes and allows the user to spot a trend over the whole stage range. It is worth noting that with the raw data the image can be rotated making the errors easier to visualise. The arrow length needs to be multiplied by a scaling factor in order to be visible as the errors are typically at the nanometre level while the stage range is micrometres. Note that the arrows represent the positioning errors only, no stage rotations are displayed even if in many cases in this text it might give a visual impression of a rotation. The angular errors are plotted as a set of 2D arrays for a 2D stage or for a single z level measurement in the 3D stage. Plotting the three angular errors together as a map of arrows, although technically possible, would be confusing.

3.2. Test rig data processing

Using the test rig we can obtain the stage positioning errors, ideally covering the complete scanning volume. There are two possible ways to treat these data in further stage operations. We can assume that all the errors are related to random errors of stage motion, after repeated measurements of the positioner error function and data averaging, the uncertainties will be Type B. This is the safest way to prevent underestimation of stage uncertainty but could be over cautious. As an opposite approach, we can assume that the errors are completely repeatable and to use them for correction of measured

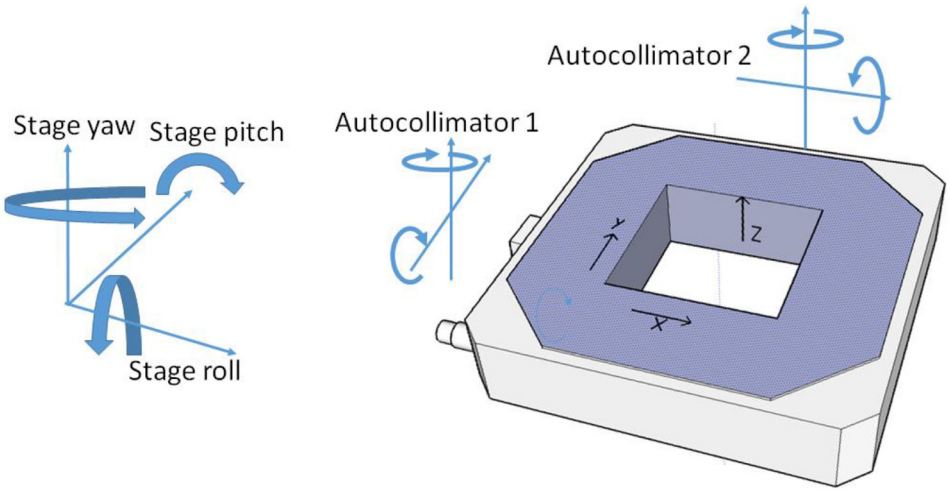

Figure 3. Stage angle definitions and autocollimators axes orientation with respect of the stage rotations.

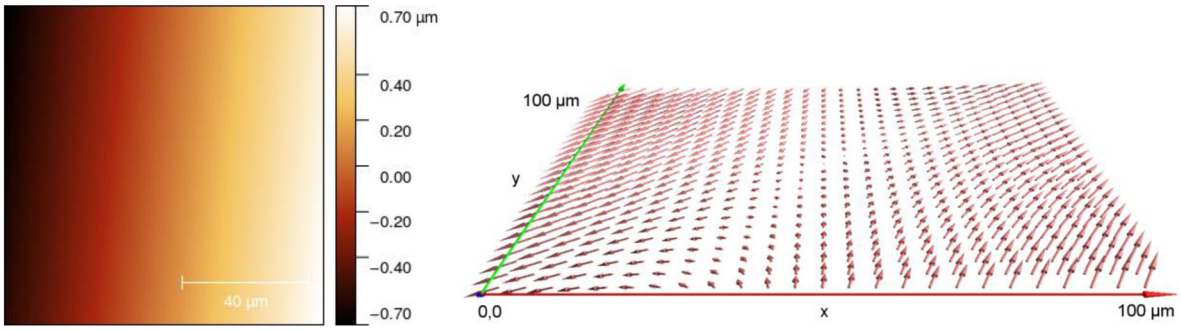

Figure 4. Data visualisation methods: (a) single axis stage errors map shown as a false colour map and (b) combined *xyz* stage errors shown in a 3D perspective view (for better visibility the length of errors shown as arrows is multiplied by 10). In both cases the scan range in x and y was 100 µm.

values. This means using the measured data directly as a lookup table for real time or offline correction of the values reported by the stage. In practice, the data analysis would be somewhere between these extrema depending on the repeatability of the system. The only way to distinguish random and systematic errors in the positioner error function is to perform repeated measurements. From the systematic errors a lookup table for corrections can be setup, either performing correction on the fly while scanning or during the data post-processing phase.

The data coming from the test rig are stored in format of the open source software for SPM data analysis Gwyddion (Nečas *et al* 2012). A separate file is created for every measurement at constant height (for *xyz* stages the individual *z* values are measured separately). Using Gwyddion all the measured data are loaded (including repeated measurements) and processed using a dedicated standalone module. The data processing is done in the following sequence.

1. Differences between interferometer and stage sensors are evaluated.
2. Differences are averaged if multiple measurements were made.
3. (Averaged) differences are rotated to minimum deviation between stage and test rig axis.
4. (Averaged) rotations are evaluated from autocollimator channels.
5. Uncertainties are evaluated: if multiple data for the same height are provided the type A uncertainty is evaluated from them. Type B type uncertainty is evaluated from local rotations (for Abbe error) and other fixed terms that are obtained from analysis outside of Gwyddion.
6. As a result, the stage errors (averaged and rotated differences between stage sensors and test rig), rotations, and a lookup table for correction of the stage position is provided.

An example of the output for five repeated scans is shown in figure 5 for the systematic errors and in figure 6 for their Type A uncertainties.

4. Uncertainty analysis

As stated earlier, traceability of the system is ensured by using optical interferometers with stabilised laser sources for position measurements and calibrated autocollimators for rotation measurements. Regarding the uncertainty budget, we are dealing with two different types of measurands from which all the lookup tables or visualisation are made. For positioning errors the basic measurand is the difference between the stage

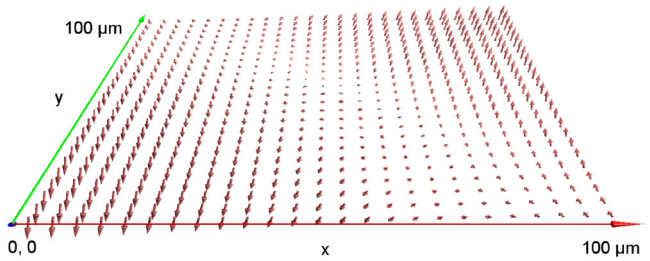

Figure 5. Averaged 2D stage positioning errors result obtained from 5 repeated scans over (100 × 100) micrometres. The length of errors shown as arrows is multiplied by factor of 10.

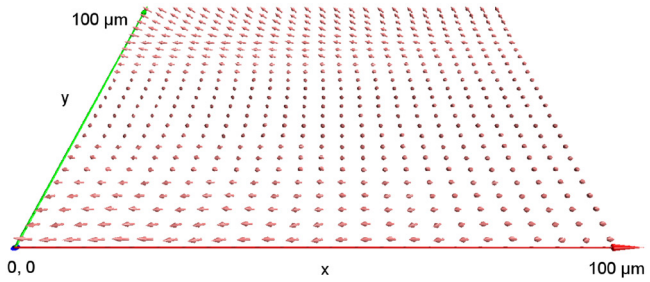

Figure 6. Type A uncertainty map of the 2D stage positioning errors result obtained from 5 repeated scans over (100 × 100) micrometres. The arrows shown are formed from x, y and z difference uncertainties, the length of arrows is multiplied by factor of 1000.

position and the real position at one point, represented by a vector of x, y, z components of the error. For rotations the basic measurand is the rotation relative to the stage orientation at centre position, represented by three values: stage pitch, roll and yaw.

The uncertainties are evaluated for each measurement individually, so it is not possible to give a single value covering all the cases. The uncertainties for measurements reported in this paper were a maximum of 5.5 nm for stage positioning errors determination and 0.25 to 2 µradians for stage rotations.

The following uncertainty contributions were considered for the stage positioning error measurements (and results evaluated from them):

4.1. Interferometer uncertainty

This comprises terms for the laser frequency, the refractive index of air, the accuracy of the fringe counting system, and interferometer non-linearity. The combined standard uncertainty associated with the interferometers is 0.5 nm for the lateral (x and y) axes and 0.6 nm for the vertical axis. The length dependent terms have an uncertainty of 1 part in $10^{-8}\,L$ (excluding dead path; see later) so for a 100 µm translation they can be ignored for the stage results presented in this paper. It should be noted that this small uncertainty is achieved only because the refractive index of air is continually measured and effective wavelength updated.

Refractive index error also contributes to a dead path error which is different for each axis and for each stage under evaluation. The temperature stability inside the enclosure is ~10 mK or better and the dead path errors have been calculated to be (dead path × 9.64 × 10^{-12} m).

4.2. Rotational errors contributing to length scale errors

These can be divided into three groups: non-orthogonality of the coordinate system, cosine errors and Abbe errors.

Non-orthogonality of the coordinate system includes non-orthogonality of the mirror and roughness of the mirror surface. The combined effect of these is $12.7 \times 10^{-7}\Delta X\Delta Y$ so for a 100 micrometre movement in X and Y, the uncertainty would be 1.27×10^{-14} m.

Cosine errors occur when there is an angular misalignment between the scan axis and measuring axis resulting in a foreshortening of the distance measured. Ideally the stage would be rotated with respect to the cube (and interferometers) until crosstalk is minimised and optimum alignment achieved. In reality this would be very difficult and is unrealistic. The cube was aligned to the frame of the stage (parallel to the x axis) using a Type B set square that conformed to BS 939:2007. This is probably what most end users would do. The angular error associated with set square is 33 micro radians. The collected data was rotated to minimise the crosstalk between the axes. This would correct for the misalignment of the precision cube mirror with respect to the interferometers and also the misalignment of scan axes to the stage body.

There is still an uncertainty associated with this process. Contributors include the alignment with the set square, and the alignment of the interferometer mirrors and the laser to the interferometer; the latter being the most dominant and the sum being $8.83 \times 10^{-8}\,L$. For a 100 µm travel this corresponds to 0.01 nm.

Abbe errors result from unwanted angular motion of the stage and the measurement plane not being coincident with the plane of motion. In the ideal case the measurement plane should be coincident with the plane of motion. In reality, the user does not know where the sensors are in the stage, there is always an offset between the sensors and the top of the stage where the object to be moved is placed leading to an Abbe error. To overcome this we have specified the height of the interferometer beams above the stage when making a measurement. If the end user works at this level, then Abbe errors will be reduced greatly since they will be given by the error in determining the height at which measurements are made and the angular error. The uncertainty associated with the height is ~0.5 mm. For practical purposes a series of calibrations could be made at different heights since the interferometer heights are adjustable.

Thermal drift: two approaches are possible. The first is to estimate based on the material components and the measured temperature change. A more pragmatic and perhaps more realistic estimate can be obtained from drift measurements of the stage under examination. This however, would yield a combined drift term for the thermal drift of the stage and rig, together with any drift in the positioning sensors and interferometers. Typical measurements made by holding the stage stationary and measuring its position using the interferometers

Table 1. Listing sources of uncertainty.

Uncertainty source	Standard uncertainty	For a 100 μm displacement
Interferometer X	0.5 nm	0.5 nm
Interferometer Y	0.6 nm	0.6 nm
Interferometer Z	0.6 nm	0.6 nm
Dead path (Dp) 150 mm	$150 \times 10^{-3} \times 9.64 \times 10^{-9}$	1.5 nm
Non orthogonality of coord. system	$12.7 \times 10^{-7}\ \Delta X \Delta Y$	1.27×10^{-14} m
Cosine error	$8.83 \times 10^{-8}\ L$	0.01 nm
Abbe error	5×10^{-3} angular error	5×10^{-3} angular error
Thermal drift	<5 nm	<5 nm
Autocollimator	0.2 μrad	0.2 μrad
Autocollimator drift	0.1 μrad h^{-1}	0.1 μrad h^{-1}

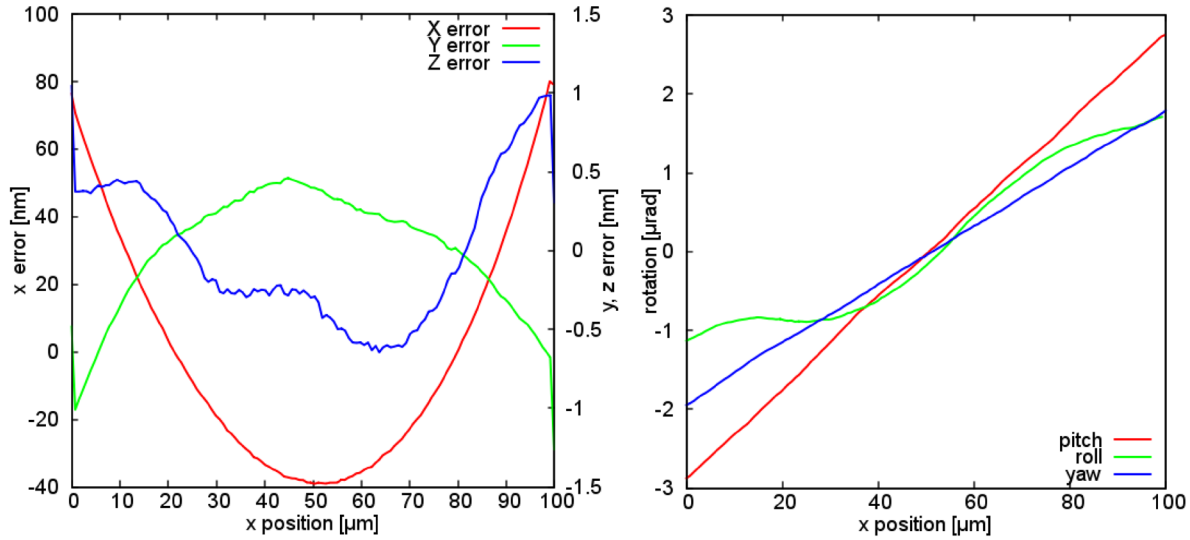

Figure 7. (a) and (b) 1D stage results: figure (a) x, y and z error after linear component removed, figure (b) stage rotations.

show that drift results during a scan are less than 5 nm and are linear. The drift encountered will be stage dependent and depend on the time taken to examine the stage.

4.3. Autocollimators and stage rotation

The following uncertainty contributions contribute towards the measurements of stage rotation (stage pitch, yaw and roll) using the autocollimators.

Autocollimator uncertainty: this comes from the calibration certificate of the autocollimator, the expanded uncertainty value is 0.2 μrad for the most sensitive scale of the autocollimator that was predominantly used.

Axes rotation inside stage: as we define rotational errors to be zero at the centre position, the potential rotation of the linear guidance system with respect to the stage frame is not measured and does not contribute to the uncertainty i.e. we are treating the stage as a black box.

Drift effects on stage rotation: this value is estimated from repeated measurements and from measurements with stage switched off. The value of the drift is less than 0.1 μrad h^{-1}.

Although variations in flatness of the mirror surface will cause an error, given that the autocollimator beam is several millimetres wide and the range of travel of the stage is typically a few hundred micrometres, the variation in mirror flatness makes no significant contribution to uncertainty in the measurement of angular motion.

A summary of these sources of uncertainty is shown in table 1.

5. Results and discussion

To illustrate the performance of the stages we start here with commercial stages, showing some of the stage errors and rotations. Errors in the 1D stage are shown in figures 7(a) and (b). A significant scale error of 1% was found which has been removed to highlight the higher order effects.

Secondly, data from the 2D stage are shown in figures 8(a) and (b), showing the positioning errors as they were measured and after subtracting the scale error, which was again not negligible (about 0.8%). The nonlinearity error was below 0.05%, which is slightly above manufacturer specifications. We can see that the major non-linearity terms are at the scanning area edges.

Thirdly, the nanopositioning stage errors and rotations from the 3D stage are shown in figure 9, for a single z level. The plotted data are shown after removing the linear part of the positioning error, if they had been included, they would

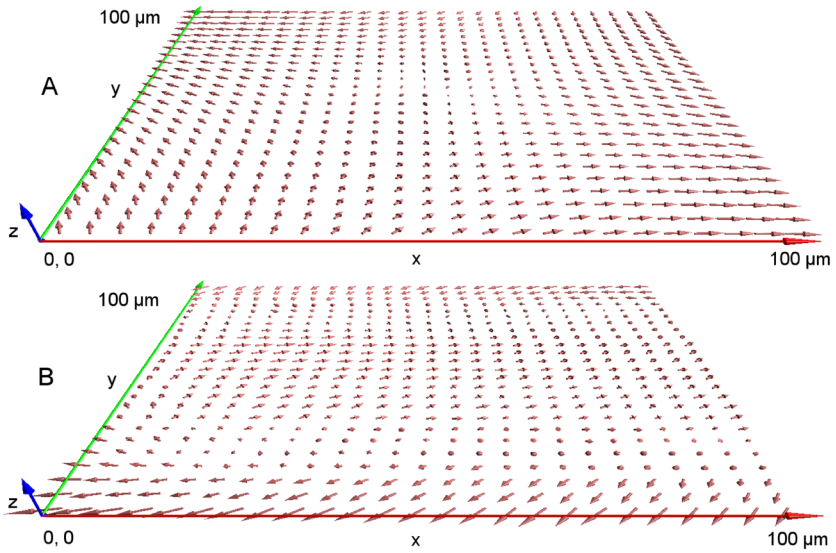

Figure 8. (a) and (b): 2D stage results: x, y and z error in 3D perspective view, (a) including the scale error, arrow lengths magnified 10× and (b) including only the nonlinear terms, arrow lengths magnified 250×.

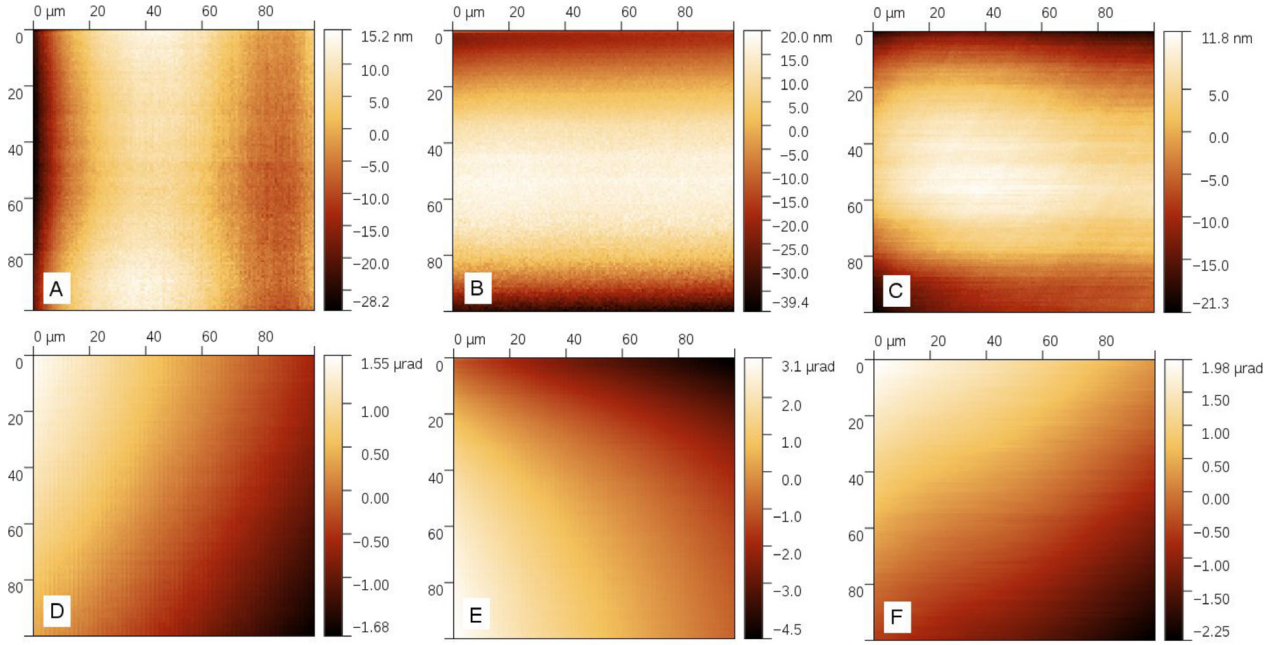

Figure 9. 3D stage results: (A) x axis error, (B) y axis error, (C) z axis error, (D) pitch, (E) roll and (F) yaw, shown for single z level in the centre of the z range.

have been, up to 300 nm (0.3% of the travel range). The non-linear part of the error is up to 0.06%, which is above manufacturer specifications. However, similar to the 2D stage, the maximum error is, as expected, at the stage positioning volume boundaries; if we would use only the central 80% of the total scanning range, the non-linearity would drop below 0.02%. As discussed in the uncertainty analysis section, all these values are valid for a particular height of the reference point above stage (due to Abbe errors), so it is important to characterize the stage at conditions as close to the practical use as possible. The stage rotations are within a few microradians which corresponds to typical stage specifications.

Finally, the plastic stage was analysed to show that the system is capable of handling more unpredictable scanning systems. Some of the errors obtained in the closed loop operation regime are shown in figure 10. It can be seen that, as expected, the errors are much higher than for any of the other stages investigated. Test rig data were used to calibrate the scale of the stage, so only the non-linear part of the error is shown. If a lookup table based on test rig data was used we could attempt to correct for the non-linear part as well, however the non-linear part of the errors is of quite random nature. From analysis of the results, the stage design could also be further optimised. It can be seen that there is a significant parasitic motion in z which could be reduced by making the linear

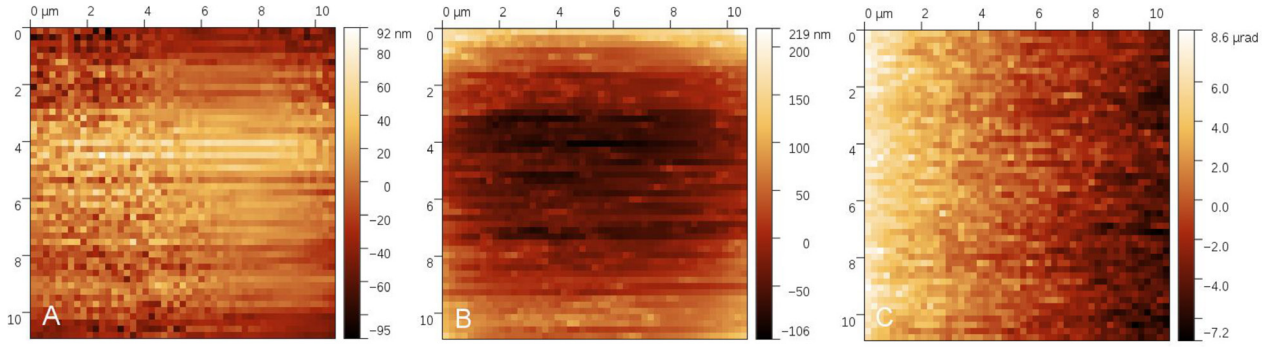

Figure 10. Plastic stage results: (A) *x* axis error, (B) *z* axis parasitic motion and (C) yaw rotational error.

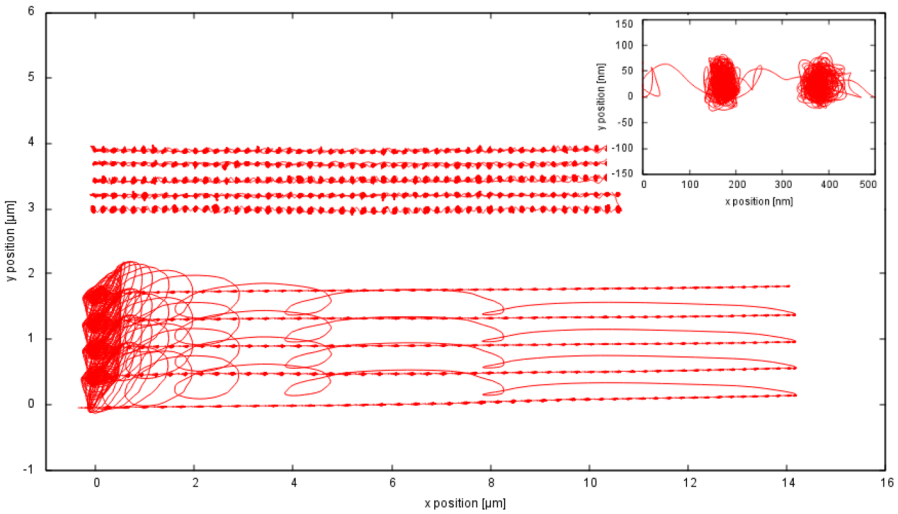

Figure 11. Plastic stage results: dynamic measurements of the closed loop (top) and open loop (bottom) regime performance, *xy* stage positions as read by interferometers shown (only first five profiles of the full range scan). Inset shows a detail of the closed loop operation for two stage positions.

guidance system stiffer, e.g. by increasing the ratio between the width of flexures and flexure joints. On the other hand, we can see that the yaw rotational error is surprisingly low, so the flexure geometry is adequate.

As mentioned above, the system was mostly designed for measuring static stage errors (in move/stop scanning regime). However, as the data are simultaneously sampled, it can be used for dynamic measurements. This is illustrated by the plastic stage data in open loop and closed loop operation shown in figure 11. The large improvement while using closed loop regime is expected. Moreover, it can be seen that the feedback loop increases the noise at individual stage positions. This is mostly related to the limited AD and DA converter resolution of the Arduino controller (12 bit), but it could be further optimized by averaging on the input side and signal dithering on the output side.

6. Conclusions

We have presented a test rig for positioning stages characterisation which is a dedicated system for traceable measurements of stage. The system was designed to provide traceable measurements with uncertainty low enough to characterize the highest accuracy stages available in the market, however, as shown, it can also be used to improve the performance of much cheaper and simpler scanning systems.

The main benefit of the test rig is that it can be used for manufacturer independent characterisation of positioning stages with known and adjustable experimental settings (e.g. reference point height above stage surface) which is more akin to the actual conditions under which the stage will be operated. This can significantly reduce some of the uncertainties when the stage is used under the same conditions. We can also analyse other error sources than those typically displayed on data sheets in both static and dynamic modes.

We have found that the stages errors can be higher (even if not dramatically) than quoted values. This can be related to stage mounting or to the selection of the reference point for measurement. However, the same issues will occur when the stage is used in practice, so it is important to have tools to check the stage performance in a set up similar to the final configuration in which the stage will be used.

The aim of this paper was to indicate how a stage may perform outside of a test environment rather than to highlight the performance of a particular stage. We also give some guidance on specifying stage performance to enable users to understand the characteristics of a stage. Some indication of how a stage was calibrated and at which height the calibration

was performed in relation to the position of the stage sensors would be useful. Due to the inherent angular errors of nanopositioning stages, there will be an Abbe error and the calibration would only be valid if the user mounts whatever they are trying to move at the same position used in the calibration. Some mention of any axis crosstalk could also prove helpful to end users, along with the relation of all angular errors quoted to a single axis.

Acknowledgments

The research was supported by EURAMET joint research project 'Metrology for movement and positioning in six degrees of freedom' receiving funding from the European Community's Seventh Framework Programme, ERA-NET Plus, under Grant Agreement No. 217257 and by project CEITEC 2020 under No. LQ1601. This project has also received funding from the EMPIR programme project 'Traceable three-dimensional nanometrology' co-financed by the participating States and from the European Union's Horizon 2020 research and innovation programme. This project has also received funding from the Institutional Subsidy for Long-Term Conceptual Development of a Research Organization granted to the Czech Metrology Institute by the Ministry of Industry and Trade of the Czech Republic.

The NPL design office and Workshop are thanked for their help with the design and construction of the test rig.

Disclaimer

The naming of any manufacturer or supplier by CMI or NPL in this scientific journal shall not be taken to be either CMI's or NPL's endorsement of specific samples of products of the said manufacturer, or recommendation of the said supplier. Furthermore, CMI and NPL cannot be held responsible for the use of, or inability to use, any products mentioned herein that have been used by them. EURAMET is not responsible for any use that may be made of the information contained in this paper.

ORCID iDs

Andrew Yacoot https://orcid.org/0000-0001-6740-821X
Miroslav Valtr https://orcid.org/0000-0002-7628-9184

References

Birch K P 1990 Optical fringe division with nanometric accuracy *Precis. Eng.* **12** 195–8
Birch K P and Downs M J 1993 An updated Edlen equation for the refractive index of air *Metrologia* **30** 152–62
Birch K P and Downs M J 1994 Correction to the updated Edlen equation for the refractive index of air *Metrologia* **31** 315–16
BS 939:2007 *Engineers' Squares (Including Cylindrical and Block Squares)* (British Standards' Institute)
Corbett A D, Shaw M, Yacoot A, Jefferson A, Schermellah L, Wilson T, Booth M and Salter P S 2018 Microscope calibration using laser written fluorescence 2018 *Optics Express* **26** 21887–99
Gillmer S R, Smith R C G, Woody S C and Ellis J D 2014 Compact fiber-coupled three degree-of-freedom displacement interferometry for nanopositioning stage calibration *Meas. Sci. Technol.* **25** 075205
Heydemann P L M 1981 Determination and correction of quadrature fringe measurement errors in interferometers *Appl. Opt.* **20** 3382–4
ISO 1:2016 *Geometrical Product Specifications (GPS)—Standard Reference Temperature for the Specification of Geometrical and Dimensional Properties* (International Organization for Standardization) (www.iso.org/standard/67630.html)
Klapetek P, Nečas D, Campbellová A, Yacoot A and Koenders L 2011 Methods for determining and processing 3D errors and uncertainties for AFM data analysis *Meas. Sci. Technol.* **22** 025501
Lazar J, Klapetek P, Číp O, Čížek M and Šerý M 2009 Local probe microscopy with interferometric monitoring of the stage nanopositioning *Meas. Sci Technol.* **20** 084007
Leach R K *et al* 2011 The European nanometrology landscape *Nanotechnology* **22** 062001
Lee C B, Lee S-K and Tarbutton J A 2014 Novel design and sensitivity analysis of displacement measurement system utilizing knife edge diffraction for nanopositioning stages *Rev. Sci. Inst* **85** 095113
Liu C-H, Jywe W-Y, Jeng Y-R, Hsu T-H and Li Y-T 2010 Design and control of a long-traveling nano-positioning stage *Precis. Engg.* **34** 497–506
Manske E, Hausotte T, Mastylo R, Machleidt T, Franke K-H and Jäger G 2007 New applications of the nanopositioning and nanomeasuring machine by using advanced tactile and non-tactile probes *Meas. Sci. Technol.* **18** 520
Manske E, Jäger G, Hausotte T and Füßl R 2012 Recent developments and challenges of nanopositioning and nanomeasuring technology *Meas. Sci Technol.* **23** 074001
Nečas D and Klapetek P 2012 Gwyddion: an open-source software for SPM data analysis *Cent. Eur. J. Phys.* **10** 181–8
Taniguchi N 1983 Current status in, and future trends of, ultraprecision machining and ultrafine materials processing *CIRP Ann.—Manuf. Technol.* **32** 573–82
Torralba M, Valenzuela M, Yagüe-Fabra J A, Albajez J J and Aguilar J J 2016 Large range nanopositioning stage design: a three-layer and two-stage platform *Measurement* **89** 55–71
Xu M, Dziomba T, Dai T and Koenders L 2008 Self-calibration of scanning probe microscope: mapping the errors of the instrument *Meas. Sci. Technol.* **19** 025105
Yacoot A and Downs M J 2000 The use of x-ray interferometry to investigate the linearity of the NPL differential plane mirror optical interferometer *Meas. Sci. Technol.* **11** 1126–30
Yacoot A, Koenders L and Wolff H 2007 An atomic force microscope for the study of the effects of tip sample interactions on dimensional metrology *Meas. Sci. Technol.* **18** 350–9